Available online at www.sciencedirect.com
ScienceDirect
Trans. Nonferrous Met. Soc. China 32(2022) 2681−2695
Transactions of Nonferrous Metals Society of China
www.tnmsc.cn

Influence of operation number on arc erosion behavior of Ag/Ni electrical contact materials

Run-zhang HUANG[1], Guo-fu XU[1,2], Qiong WU[1], Meng YUAN[1], Chun-ping WU[1,2]

1. School of Materials Science and Engineering, Central South University, Changsha 410083, China;
2. Key Laboratory of Nonferrous Materials Science and Engineering of Ministry of Education, Central South University, Changsha 410083, China

Received 28 July 2021; accepted 30 June 2022

Abstract: Arc erosion behavior of Ag/Ni materials with different operation numbers was investigated by OM, 3DOP and SEM. The results indicated that the arc erosion of Ag/10Ni electrical contact material fabricated by sintering−extrusion technology was more and more serious with the operation numbers increasing from 1000 to 40000. With the same operation numbers, the arc erosion on anode was more serious than that on cathode. Besides, the pores preferred to emerge around the arc effect spot during the first 10000 operations. And the morphology of the molten silver on cathode and anode was different due to the action of gravity and arc erosion. Furthermore, the relationships among arc energy, arc time, welding force, electric resistivity, temperature and mass change on contacts were discussed, which indicated that the mass loss on cathode was mainly caused by the fracture of molten bridge.
Key words: Ag/Ni electrical contact material; operation number; arc erosion; arc parameter

1 Introduction

Ag-based electrical contact materials are widely used as the key part of electrical apparatus due to their low electrical resistivity and high thermal conductivity. Ag/CdO is the most popular and outstanding Ag-based electrical contact material. However, it has been proven to be extremely harmful to human health and natural environment [1−3]. Therefore, the research and development of cadmium-free environment-friendly alternative contact materials are urgent, and have begun to receive widespread attention in the academic and industrial fields.

In order to displace Ag/CdO electrical contact materials, researchers have designed and developed a variety of Ag-based electrical contact materials, such as Ag/SnO_2, Ag/C and Ag/Ni [4]. Ag/Ni electrical contact materials have been widely used in the field of household appliances, contactors, miniature circuit breakers and automobile relays due to their low and stable contact resistance, outstanding processability and environmental friendliness [5−7]. In particular, the dissolution and precipitation of Ni phases can play an important role in dispersing the arc and preventing concentrated erosion under the condition of low current [7]. Hence, Ag/Ni contacts are usually used in the load conditions of 50−100 A and below [8,9]. However, Ag/Ni electrical contact materials are prone to material transfer and welding when exposed to high current, especially surge current, which results in their shortage of arc erosion resistance [10−12]. Therefore, how to improve the welding resistance of Ag/Ni electrical contact materials and expand their service current range have become the focus of research [13−15].

Corresponding author: Chun-ping WU, Tel: +86-731-88877862, E-mail: Chunpingwu@csu.edu.cn
DOI: 10.1016/S1003-6326(22)65975-2

The additives can improve and enhance the arc erosion resistance of silver-based electrical contact materials [16,17], and the effects of additives on arc erosion of Ag/Ni electrical contact materials were investigated. LI et al [7] found that the addition of carbon allotropes could improve the welding resistance of Ag/Ni electrical contact materials. YANG et al [18] found that the addition of metal oxides (MeO) could improve the voltage resistance and hardness of Ag/Ni electrical contact materials.

In addition, the influence of Ni morphology on arc erosion behavior was investigated in order to improve the arc erosion resistance of Ag/Ni electrical contact materials. LIN et al [19] found that the pinning effect of fibrous Ni was better than that of granular shape on maintaining the stability of the molten pool, but the fibrous Ni was easily affected by thermal effect and turned into particles again. LIN et al [20] also found that the Ni-belt could enhance the physical properties of Ag/Ni electrical contact materials. LI et al [15] found that Ni-rich phases were easily to cause arc erosion on anode surfaces.

Arc erosion is a very complex physical phenomena, which is related to many factors, such as electrical factors, material factors, mechanical factors and environmental factors. Operation number is an important electrical factor affecting arc erosion. In our previous works, the influence of operation number on arc erosion of Ag/CuO, Ag/ZnO and Ag/CdO electrical contact materials was investigated [17,21,22]. It can be found that the operation number had different influence on the arc erosion of silver-based electrical materials with different additions. However, the influence of operation number on arc erosion of Ag/Ni electrical contact materials has not been reported yet. In particular, the formation mechanism of arc erosion morphology of Ag/Ni electrical contact materials is still unclear. In this work, the electrical contact physical phenomena, the macro and micro arc erosion morphology, the arc erosion microstructure on cross section of Ag/10Ni electrical contact materials after 1000−40000 operations were characterized. In addition, the relationships between arc energy, arc time and resistivity were discussed, the relationships between mass loss, temperature rise and welding force were explained, and the formation processes of pore and molten silver were also analyzed.

2 Experimental

2.1 Tested contacts

Ag/Ni (Ag: 90 wt.%; Ni: 10 wt.%) electrical contact materials fabricated by sintering−extrusion (SE) technology were selected as samples. The form, contact mode and optical microstructure of Ag/Ni electrical contact materials were the same as those in our previous research [5], but the movable contacts had a curved surface and the stationary contacts had a flat one in this work.

2.2 Experimental conditions

Apparatus of electrical lifespan test used in this work was the same as that in our previous research [5], where the experimental conditions are given in Table 1. Electrical contact physical parameters including arc energy (E), arc time (t), welding force (F), electrical contact resistance (R) and temperature (T) were measured during the arc operation. Three contact samples were tested for considering the repeatability of experimental results, and the basic physical properties are listed in Table 2.

Table 1 Experimental conditions

Parameter	Value or description
Contact material	Ag/10Ni (Ag: 90 wt.%; Ni: 10 wt.%)
Circuit condition	DC 19 V, 20 A, inductive load
Frequency/Hz	0.67 (ON 0.3 s)
Number of operations	1000, 3000, 5000, 10000, 20000, 30000, 40000
Switching mode	DC
Contact force/N	0.98
Surrounding gas	Air
Minimum arc voltage/V	10
Minimum arc current/A	0.7
Electrode spacing/mm	2

In this work, the mass loss was measured with an electronic scale. The optical microstructure was characterized by optical microscope (POLYVAR-MET). Three-dimensional topography and profile data at center point of Ag/10Ni electrical contact materials after arc erosion were measured with a three-dimensional surface topography measurement

Table 2 Physical properties of Ag/10Ni materials fabricated by SE technology

Density/ ($g \cdot cm^{-3}$)	Electrical contact resistance/($\mu\Omega \cdot cm$)	Hardness ($HV_{0.3}$)	Strength of extension/MPa	Elongation after fracture/%
10.27	1.88	95	350	13

instrument (WYKO NT9100). The arc erosion morphology was characterized with a scanning electron microscope (Sirion 200).

3 Results

3.1 Physical phenomena of electrical contact

The average values of arc energy ($\overline{E}$), arc time ($\overline{t}$) and welding force ($\overline{F}$) of Ag/10Ni electrical contact materials with different operation numbers are represented in Fig. 1(a), where the changing tendency of $\overline{E}$ is similar to $\overline{t}$ with different operation numbers. This result is consistent with our previous published work [5], and conforms to the relationship described by Eq. (1) as well. In addition, $\overline{E}$ and $\overline{t}$ reach the peak values (711.3 mJ and 8.981 ms) when the operation number is 40000. Besides, the changing tendency of $\overline{F}$ is different from $\overline{E}$ and $\overline{t}$ with different operation numbers, and $\overline{F}$ reaches the peak value (11.81 g) when the operation number is 30000 rather than 40000.

$$E = \sum UIt \tag{1}$$

where U, I and t refer to the voltage, current and arc time of the arc emerged on the apparatus.

The changes of electrical resistivity (ΔR) and temperature (ΔT) of Ag/10Ni electrical contact materials after different operation numbers are presented in Fig. 1(b), where their variation tendency fluctuates with the increase of the operation number. ΔR value is the minimum when the operation number is 10000 and is the maximum when the operation number is 40000. ΔR value is the minimum when the operation number is 10000 and is the maximum when the operation number is 30000.

The mass changes on cathode (Δm_-) and anode (Δm_+), and total mass change of Ag/10Ni electrical contact materials after different operation numbers are presented in Fig. 1(c). The total mass of Ag/10Ni electrical contact materials after different operation numbers decreases except for 3000 operations. The mass on anode is reduced after different operation numbers, while that on cathode

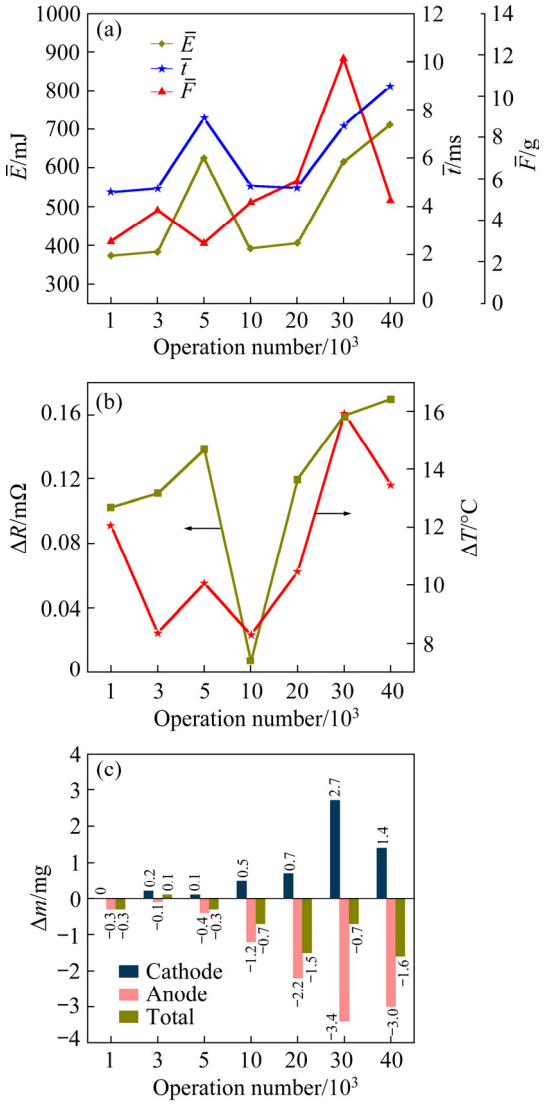

Fig. 1 Arc parameters of Ag/10Ni electrical contact materials with different operation numbers: (a) Average values of arc energy, arc time and welding force; (b) Change of electrical resistivity and temperature; (c) Mass change on cathode, and anode, and total mass change

is increased except for 1000 operations. It is indicated that the mass of Ag/10Ni electrical contact materials during operation is transferred from anode to cathode. As for the feature that mass does not change on cathode with 1000 operations, it may be resulted from a balance between the mass loss caused by molten bridge fracture and the mass gain caused by ions precipitation.

3.2 Erosion morphology of Ag/10Ni electrical contact materials

3.2.1 Macro-morphology

Three-dimensional macroscopic morphology of Ag/10Ni electrical contact materials after different operation numbers is presented in Fig. 2. With the increase of operation number, the change of three-dimensional macroscopic morphology is intensified, indicating more serious arc erosion produced on contacts' surface. Convex peaks are observed on cathode while craters can be found on anode, where both the amount and height of the convex peaks or the depth of the craters increase with the increase of the operation number. The convex peaks on cathode and the crater on anode mean that the contact mass is transferred from anode

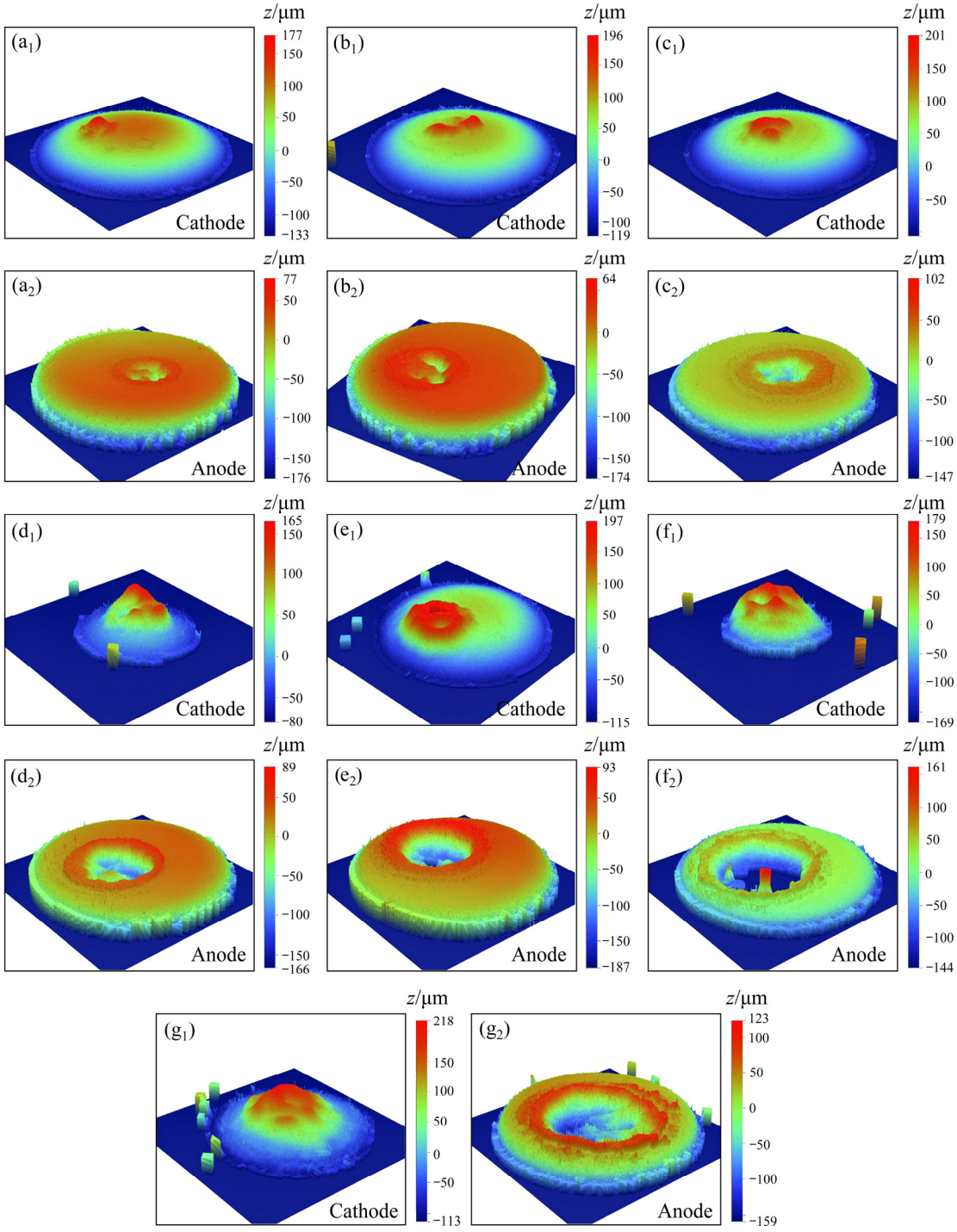

Fig. 2 Three-dimensional macroscopic morphologies of Ag/10Ni electrical contact materials after different operation numbers: (a_1, a_2) 1000; (b_1, b_2) 3000; (c_1, c_2) 5000; (d_1, d_2) 10000; (e_1, e_2) 20000; (f_1, f_2) 30000; (g_1, g_2) 40000

to cathode, which is consistent with the result of mass change in Fig. 1(c). In addition, the change of three-dimensional macroscopic morphology on anode is more serious than that on cathode after the same operation number, which indicates that the arc erosion on anode is harder than cathode erosion. Together with the mass changing result on anode and cathode, it can be concluded that the anode seems to be more sensitive to arc erosion than cathode under the same operation conditions.

3.2.2 Micro-morphology

(1) Pore

The feature of pore morphology of Ag/10Ni electrical contact materials after different operation numbers is presented in Fig. 3. It can be seen that most of the pores occur on anode, while those are observed on cathode only when the operation number is 30000. There are two kinds of erosion pore characteristics on the contact's surface. One kind of erosion pore can be observed on the surface of the molten silver (Figs. 3(a−f)), while the other can be observed on the surface of the splash products (Figs. 3(b, g, h)). The circular area of A, B and C in Figs. 3(a, c, d) surrounded by pore is presumed to be the direct contact area of the arc, which will be called as the central area later.

(2) Crack

The feature of crack morphology of Ag/10Ni electrical contact materials after different operation numbers is presented in Fig. 4. It can be seen that the cracks occur on anode at the early stage of operation while those can be observed on cathode only when the operation number is larger than 20000. In addition, the cracks on anode are Y shaped, while those on cathode are straight line shaped.

The formation process of crack can be divided into two stages: the first is the generation of the crack source and the second is the extension of the crack. The generation of crack mainly stems from pore, tiny crack, impurity, grain boundary and interface dislocation groups, since these defects are capable of weakening the surface strength. Pores can be observed around the cracks, which indicates that the pores may result in the generation of crack and guide the extending direction of the cracks (as marked in white circle in Fig. 4(b)). The result of Fig. 4 indicates that pores are more likely to be

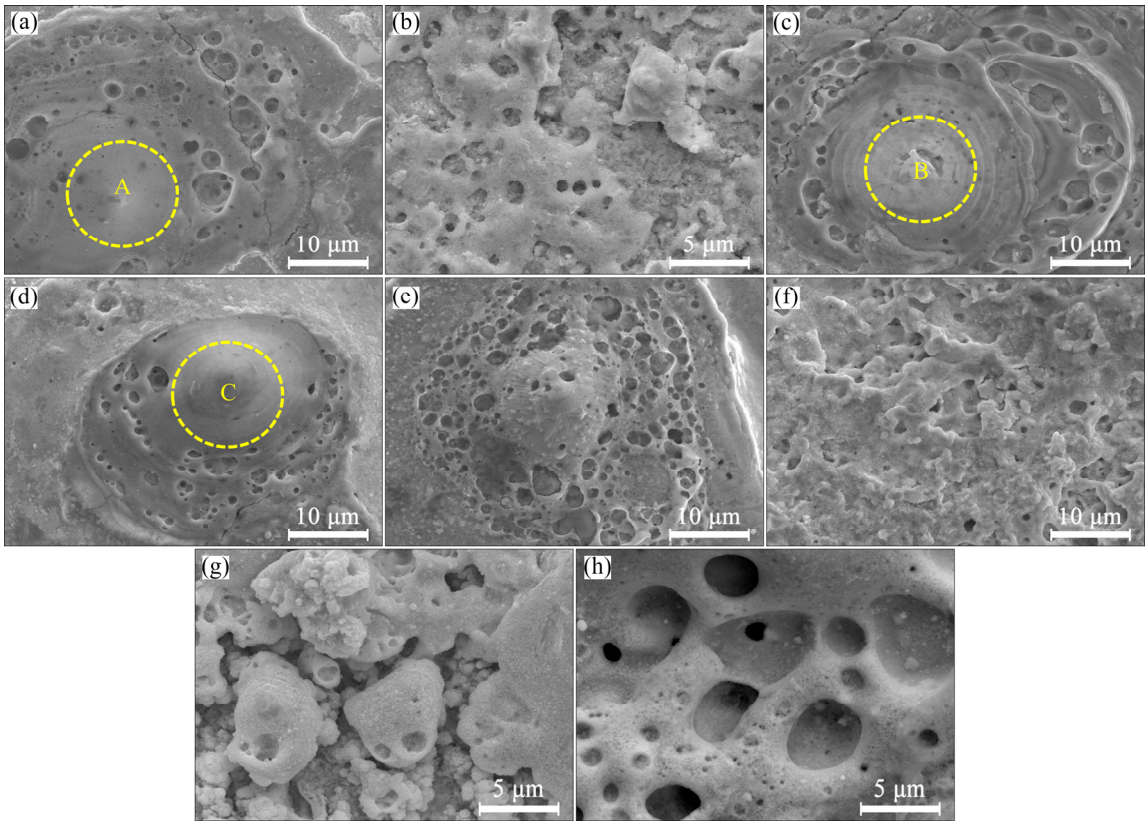

Fig. 3 Feature of pore morphology of Ag/10Ni electrical contact materials after different operation numbers: (a) 1000, on anode; (b) 3000, on anode; (c) 5000, on anode; (d) 10000, on anode; (e) 20000, on anode; (f) 30000, on anode; (g) 30000, on cathode; (h) 40000 on anode

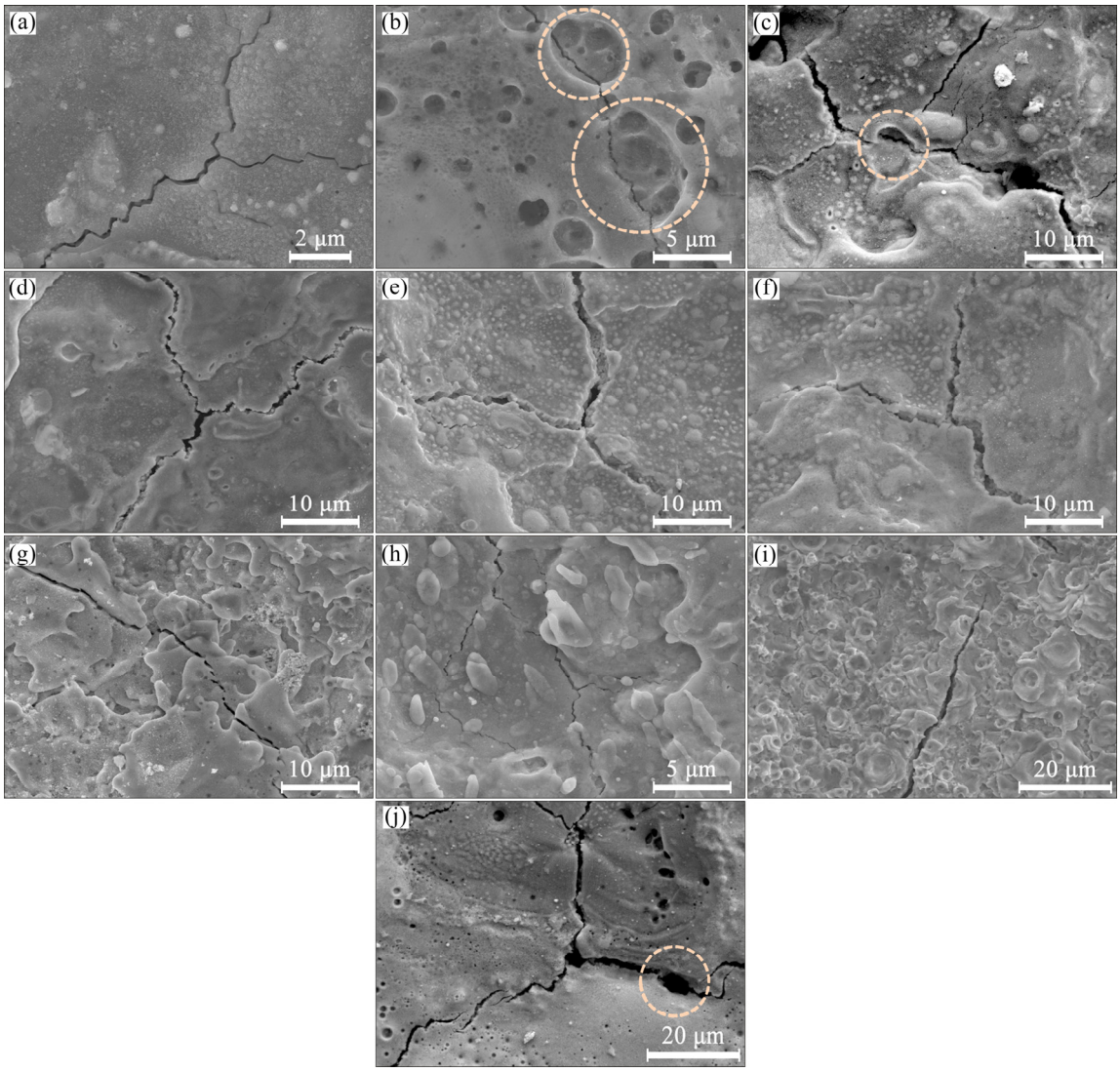

Fig. 4 Feature of crack morphology of Ag/10Ni electrical contact materials after different operation numbers: (a) 1000, on anode; (b) 1000, on anode; (c) 3000, on anode; (d) 5000, on anode; (e) 10000, on anode; (f) 20000, on anode; (g) 20000, on cathode; (h) 30000, on anode; (i) 30000, on cathode; (j) 40000, on cathode

found on anode, which should be responsible for bringing higher occurrence rate and more complex extending direction of cracks on the anode than the cathode, and also explains the reason why there are more Y-shaped cracks on anode.

(3) Molten silver

The feature of molten silver morphology of Ag/10Ni electrical contact materials after different operation numbers is presented in Fig. 5. Temperature on contacts will increase during arc action. When the temperature reaches the melting point of silver, the silver in solid state will melt into liquid and then forms molten pool on the surface. When the contacts break and the break-arc disappears, the molten silver will be forced to solidify into the shape of islands before spreading on surface, due to the rapid cooling rate.

The molten silver in the shape of tentacle is observed on anode when the operation number is 1000 (see Fig. 5(a)) and irregular protrusion is observed on anode when the operation number is 3000 (see Fig. 5(b)). The molten silver in the shape of petal is observed on cathode (see Fig. 5(c)) and irregular protrusion with droplet-like morphology is observed on anode (see Fig. 5(d)) when the operation number is 5000. The molten silver in the shape of water wave is observed on cathode (see Fig. 5(e)) and island with droplet-like morphology is observed on anode (see Fig. 5(f)) when the operation number is 10000. The molten silver in the

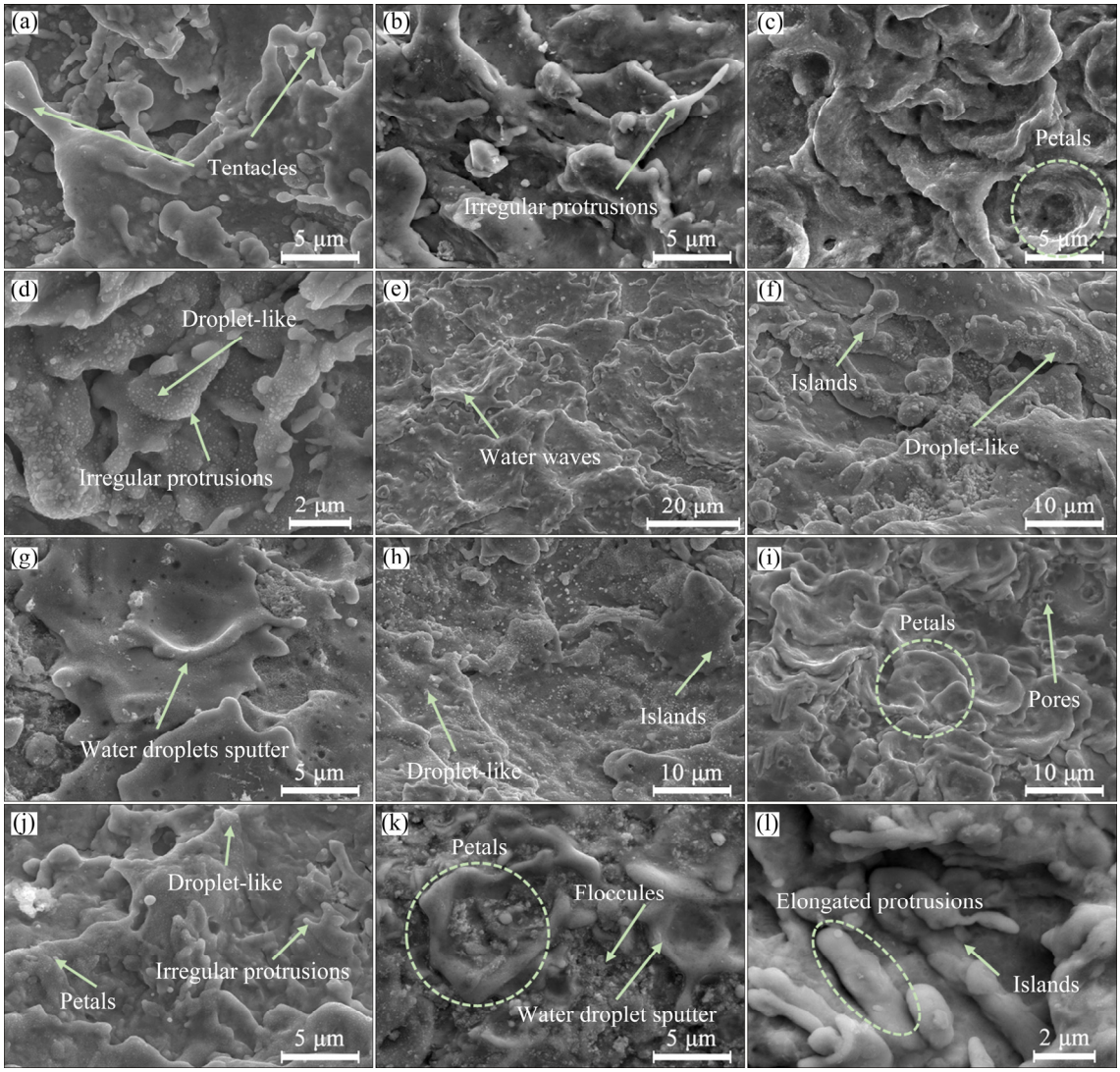

Fig. 5 Feature of molten silver morphology of Ag/10Ni electrical contact materials after different operation numbers: (a) 1000, on anode; (b) 3000, on anode; (c) 5000, on cathode; (d), 5000 on anode; (e) 10000, on cathode; (f) 10000, on anode; (g) 20000, on cathode; (h) 20000, on anode; (i) 30000, on cathode; (j) 30000, on anode; (k) 40000, on cathode; (l) 40000, on anode

shape of water droplet sputter is observed on cathode (see Fig. 5(g)) and island with droplet-like morphology is observed on anode (see Fig. 5(h)) when the operation number is 20000. The molten silver in the shape of petal with pore is observed on cathode (see Fig. 5(i)) and island with irregular protrusion and droplet-like morphology is observed on anode (see Fig. 5(j)) when the operation number is 30000. The molten silver in the shape of petal and water droplet sputter with floccule is observed on cathode (see Fig. 5(k)) and island with elongated protrusion and droplet-like morphology is observed on anode (see Fig. 5(l)) when the operation number is 40000.

Three features of the molten silver on contact surface can be concluded based on the descriptions above. First, the formation of the molten silver on the anode is earlier than that on cathode after different operation numbers. Second, the droplet-like molten silver is more common on anode than on cathode as well. Third, the shape of the molten silver on cathode is different from that on anode, where the former one can be described as layers with round plates stacked on each other, while there is more island-like molten silver with protrusions on anode. Therefore, the molten silver on cathode and anode can be named “piled plates” and “crawling islands”, respectively.

(4) Morphology of splashing product

Pore, crack and molten silver are the common arc erosion morphologies. Under the action of arc, Ni particles suspending in molten pool splash out, so does the liquid silver. Both the splashed Ni particles and liquid silver are named as “splashing product”. The morphology of splashing products of Ag/10Ni electrical contact materials after different operation numbers is represented in Fig. 6.

It can be found that the morphology of the splashing products can be specifically described as rock candy (see Figs. 6(a, b)), dense crystalline bulk (see Fig. 6(c)), floccule (see Fig. 6(d)), irregular particle (see Figs. 6(e, m, k)), cauliflower (see Fig. 6(e)), irregular aggregation (see Fig. 6(g)), spherical splash (see Fig. 6(h)), nanometer particle

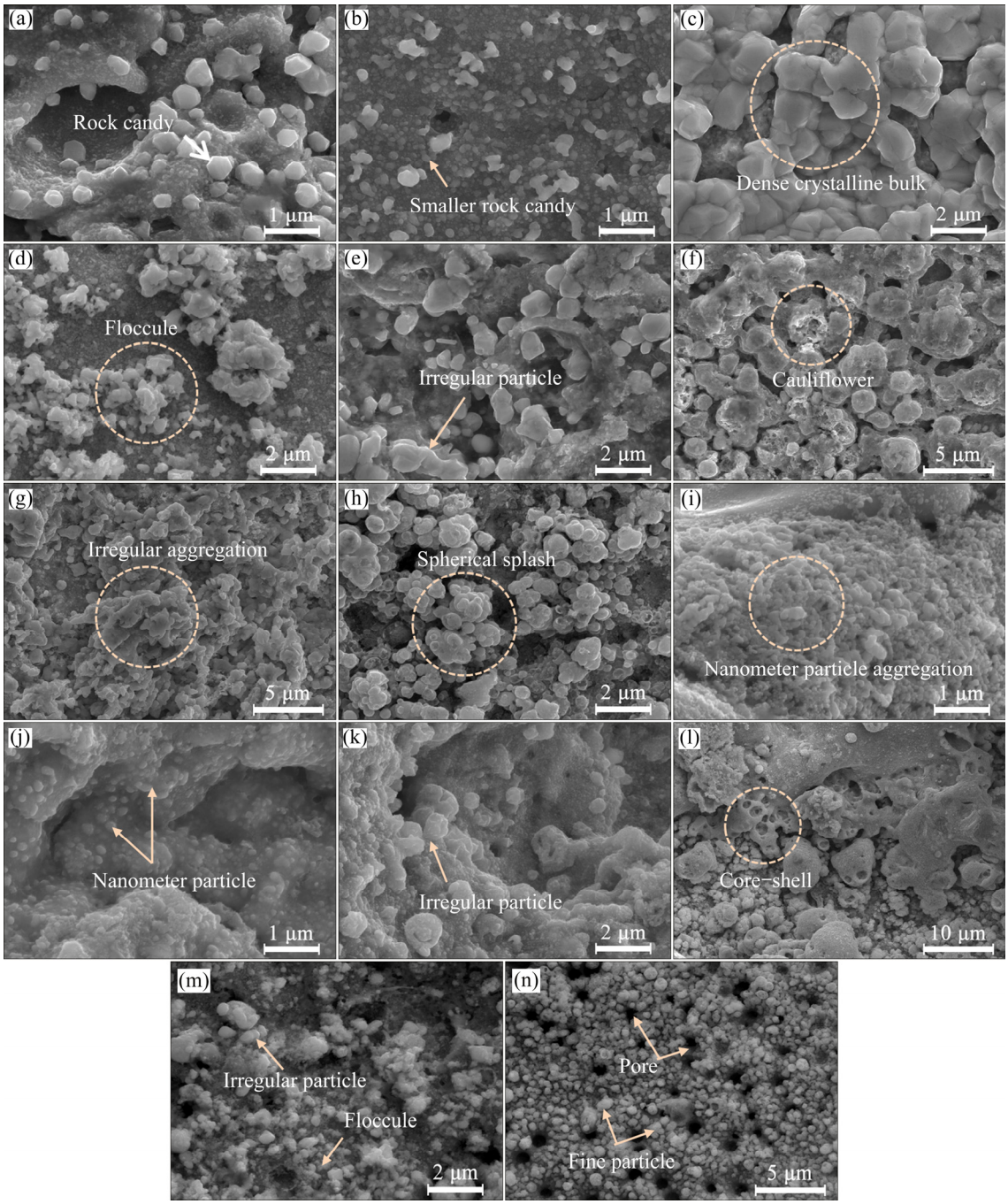

Fig. 6 Morphology of splashing product of Ag/10Ni electrical contact materials after different operation numbers: (a) 1000, on cathode; (b) 1000, on anode; (c) 3000, on cathode; (d) 3000, on anode; (e) 5000, on cathode; (f) 5000, on anode; (g) 10000, on cathode; (h) 10000, on anode; (i) 20000, on cathode; (j) 20000, on anode; (k) 30000, on cathode; (l) 30000, on anode; (m) 40000, on cathode; (n) 40000, on anode

aggregation (see Fig. 6(i)), nanometer particle (see Fig. 6(j)), core−shell (see Fig. 6(l)) and pore (see Fig. 6(n)). They can generally be divided into two kinds as "coral-like" (Figs. 6(i, l−n)) and "droplet-like" (Figs. 6(j−l)). The "droplet-like" morphology refers to shiny particle dispersed on molten silver that looks like droplet, and the formation of the "droplet-like" morphology has two ways of precipitation and splashing. The precipitation way depends on the solubility of Ni in Ag and the solubility of Ni precipitation before and after thermal effect caused by arc or electricity. These precipitated Ni particles disperse uniformly on molten silver, increase the area of interface between Ag and Ni that is easily to emit electron and makes difference in dispersing arc, which further leads to the difference in temperature locally [15]. Another formation way of the "droplet-like" morphology is the Ni splashed from another contact. The formation of the "coral-like" morphology origins from the gaseous silver and liquid silver generated from thermal effect on contact surface induced by arc. Gaseous silver moves to the interelectrode space and may run into relatively cold air, which adsorbs the heat of the metal vapor and forces it to solidify. Then, the cooled silver falls back to the contact surface, where it piles up and forms the "coral-like" morphology [5]. In addition, the molten silver during the solidification will perform size reduction, which results in the formation of the pores on the splashing product in Figs. 3(b, g, h). As for the liquid silver origin, under the action of electric field force, Lorentz force and contact pressure, the splashed molten silver moves in diverse direction from the contacts surface, one part of which falling back to the arc center will keep in the state of liquid due to the arc effect, while the other part landing at the periphery zone will solidify and pile up to have "coral-like" morphology [10].

3.3 Erosion microstructure on cross section of Ag/10Ni electrical contact materials

The optical microstructures on cross section of Ag/10Ni electrical contact materials after different operation numbers are presented in Fig. 7. When the operation number is 1000, the cross section of contacts changes little, and only a small amount of erosion products (the white arrow in Fig. 7) can be observed on cathode while the convex peak and crater are not found (see Fig. 7(a)), which indicates that only little material is transferred at the early stage of arc erosion. This result is consistent with the mass loss result presented in Fig. 1(c) as well. When the operation number is larger than 1000, the convex peak (the red square in Fig. 7) is observed on the curved cathode surface while the crater (the blue circle in Fig. 7) is observed on the flat anode surface. With the operation numbers increasing, the change of the cross section of contacts is more and more obvious, where the area of the convex peak on cathode and that of the crater on anode increase, indicating that the arc erosion of Ag/10Ni electrical contact materials is more and more serious with the increase of operation numbers.

4 Discussion

4.1 Relationship among physical parameters of electrical contact

The relationships between the temperature change (ΔT) and mass change on anode (Δm_+), average value on welding force ($\overline{F}$) and mass change on cathode (Δm_-) with different operation numbers are presented in Fig. 8. It is indicated that the variation tendency of ΔT is similar to that of Δm_+ with the same operation numbers (see Fig. 8(a)). The linear fitting result is depicted in Fig. 8(b) and the proportional relationship value (R^2) is 0.4679.

Anode is sensitive to evaporation and splash erosion due to the thermal effects. Both evaporation and splashing erosion will become more serious at high temperature, which can be explained with the relationship between ΔT and Δm_+. However, the value of R^2 as 0.4679 is insufficient to provide enough evidence for explaining that temperature may play a leading role in mass change on anode. The molten bridge fracture results in the mass change on both anode and cathode, where the mass will transport from anode to cathode since the high temperature section in molten bridge is close to anode [10]. The amount of the mass transport caused by the molten bridge fracture is sensitive to the temperature and welding force, so Δm_+ is proportional to ΔT to a certain extent, but not decided by ΔT alone.

Figures 1 and 8(c) indicate that the changing tendency of $\overline{F}$ is similar to Δm_- during each operation. The relationship between $\overline{F}$ and Δm_- is depicted in Fig. 8(d), where the proportional

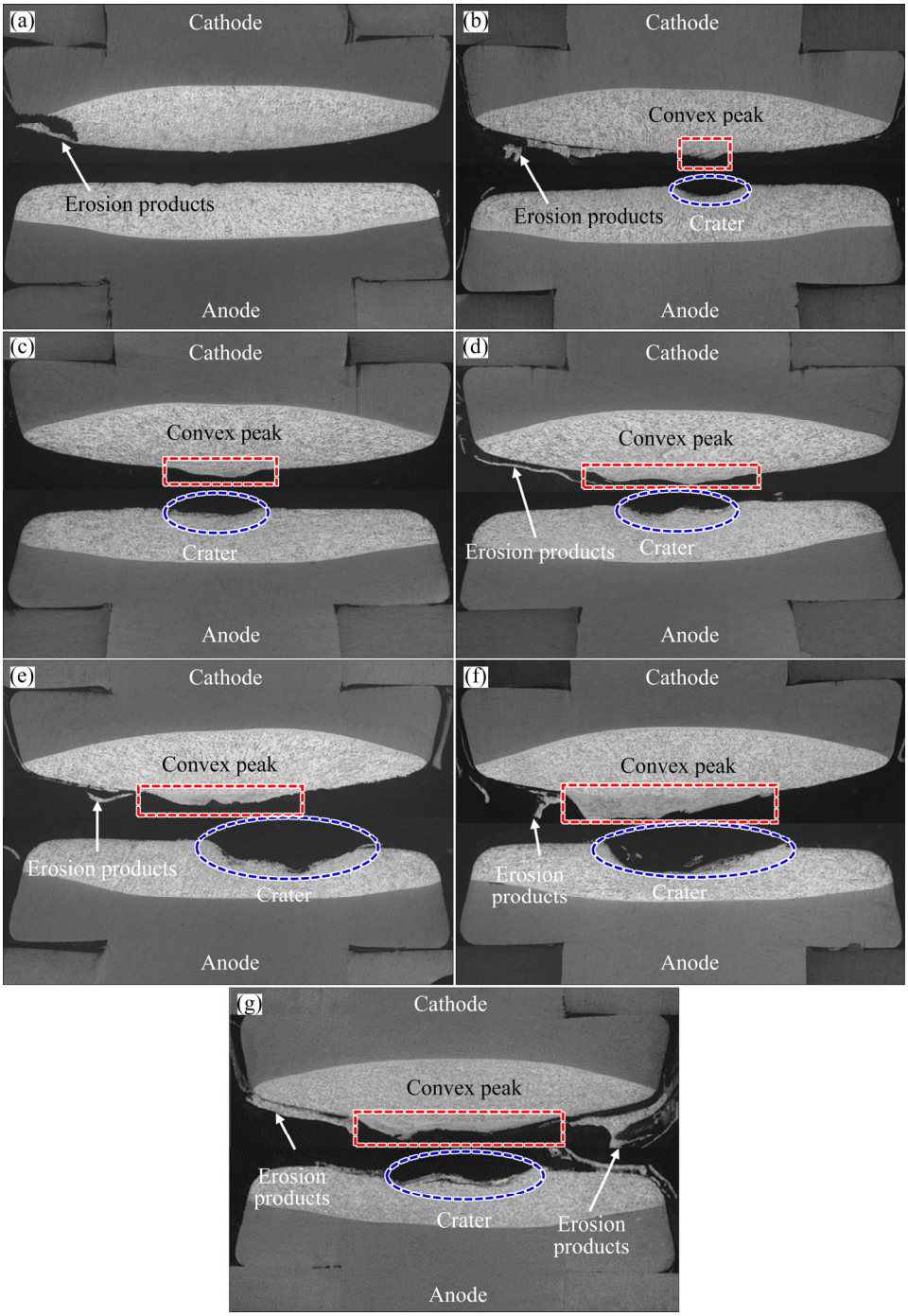

Fig. 7 Optical microstructures on cross-section of Ag/10Ni electrical contact materials after different operation numbers: (a) 1000; (b) 3000; (c) 5000; (d) 10000; (e) 20000; (f) 30000; (g) 40000

parameter (R^2) between $\overline{F}$ and Δm_- is 0.84326, larger than that between ΔT and Δm_+.

The relationship between ΔT and Δm_+ indicates that the molten bridge fracture can lead to the mass transport from anode to cathode, which is also an influence factor in Δm_-. From the numerical point of view, Δm_- is more sensitive to $\overline{F}$ than ΔT to a large extent because of the high value of R^2, but there are still other influencing factors that make difference in Δm_-, such as splashing products from anode in the form of molten silver during make-arc and break-arc (Figs. 2(a, b, d, e, g)) and deposition of metal vapor generated from evaporation on both anode and cathode. This explains why there is rather high but not total proportional relationship between $\overline{F}$ and Δm_-.

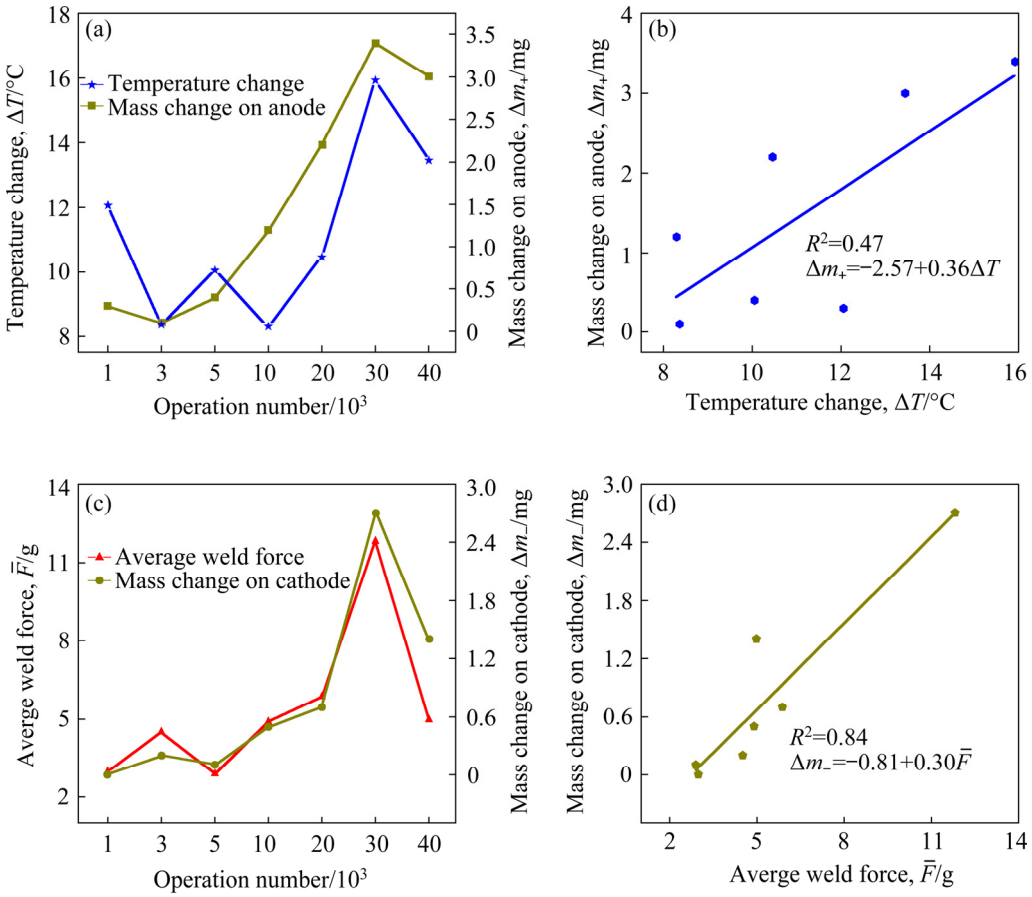

Fig. 8 Relationships between temperature change and mass change on anode (a, b), and average welding force and mass change on cathode (c, d)

4.2 Formation mechanism of arc erosion morphology

4.2.1 Formation process of pore

According to the results above, it can be found that there are circular areas where pores are rarely seen during the first 10000 operations, as presented in Figs. 3(a, c, d), in which the circular A, B, C zones are presumed to be the central zone of arc contact.

Generally, the formation process of pore can be divided into four stages that are dissolution, aggregation, escape and burst. When the anode and cathode contact partially, the temperature around the contacting spots increases, leading to the silver melting. Then, the dissolving of Ni and oxygen in silver intensifies since their solubility in liquid silver is higher than that in solid silver [5]. In addition, oxygen in air between cathode and anode may dissolve in contacts and diffuse into the inner space of it. Then, the dissolved oxygen will get together with the particles that dissolve in silver like Ni as well as any other impurity, and carry on the nucleation. Afterwards, they start growing up to become bubbles when they reach the size of nucleation by continuously absorbing surrounding oxygen. By the time the contact break and break-arc disappear, the temperature of contacts surface will drop rapidly, leading to the quick solidification of liquid silver. Meanwhile, the oxygen dissolved in liquid silver may be forced to leave the contacts because of the lower oxygen solubility in cool silver. Some of the oxygen dissolved in liquid silver cannot escape from the contacts surface for they are far to reach, and then this part remains inside the contacts in the form of pores. The other part of oxygen dissolved in liquid silver may be quick enough to escape the surface and burst due to the existence of surface tension caused by Marangoni effect [14], which not only leaves air hole on contacts surface but also leads to splashing of molten metal.

Based on the discussion above, the feature that there are circular areas of pores formed can be attributed to the special effect of arc during four

stages in pores' formation. As depicted in Fig. 9(a), the dissolution process of oxygen is different at the directly-contacting zone with arc (referred as central zone below), where the oxygen is consumed to a larger extent because of the longer arc erosion time here than that in other places, which further results in the situation that the oxygen dissolved here is still the least even though it possesses the highest temperature. The aggregation process of oxygen is depicted in Fig. 9(b), where both the action of gravity and the difference in melting point and density lead to opposite moving directions of Ag and Ni, particularly in the central zone where the temperature is the highest and silver flows most actively. Consequently, the element distribution of Ni in the central zone is more than that in periphery zone on the contact surface, and the content of oxygen is less in central zone. In addition, the size of nucleation spot contributing to the aggregated gas here is also smaller than that in any other place. The escaping process of oxygen is depicted in Fig. 9(c), where the movement of the gas bubbles toward contacts surface depends on their size and the concentration difference of oxygen in molten pool and contacts surface, which is further determined by the temperature inside and outside the contacts. The change of temperature in the central zone is less than that in the periphery zone of arc due to the long-term action of the arc in central zone. This is why the bubbles inside the central zone move slowly before reaching contacts surface and remain in the contacts even after the solidification of the molten pool. The burst process of oxygen is depicted in Fig. 9(d), where the temperature difference in the central zone is low and the surface tension may be not enough to break the smaller bubbles since the intensity of Marangoni effect decreases with the fairly lower temperature difference here. Even the busted bubbles are small enough to be filled up with the

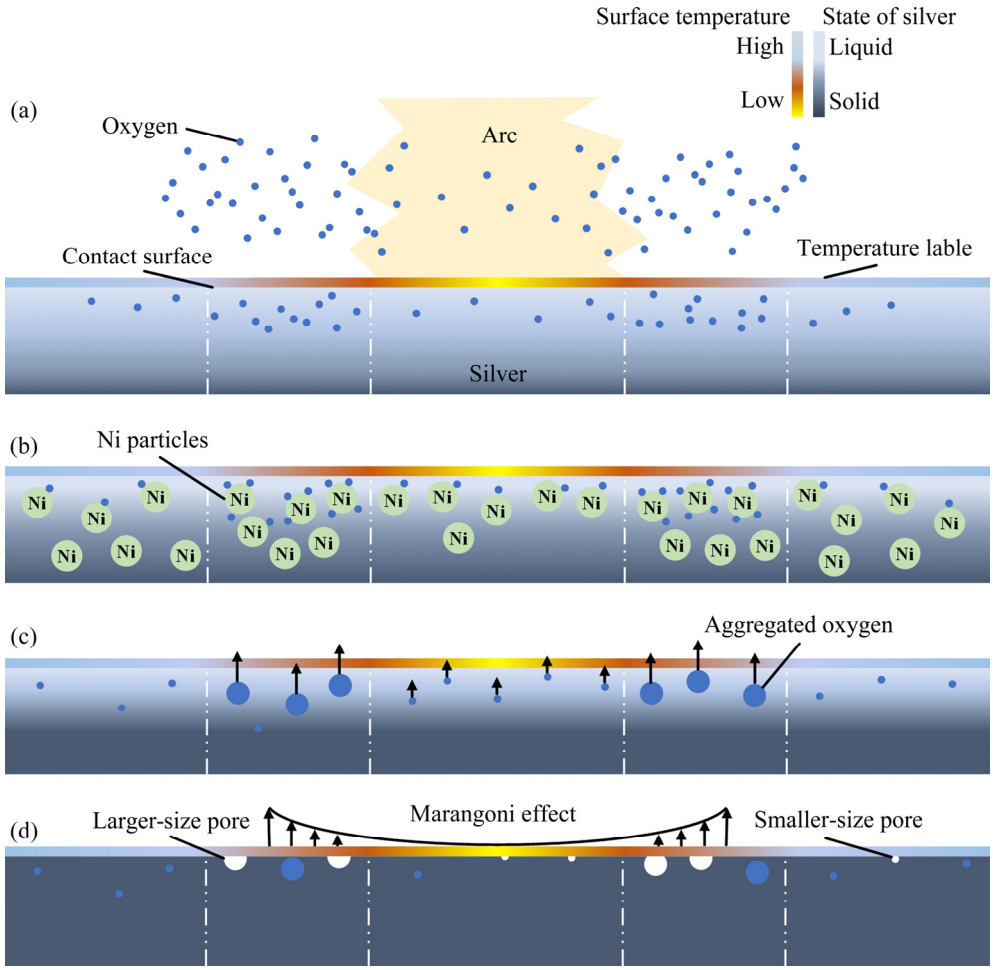

Fig. 9 Schematic of formation process of pore: (a) Dissolution of oxygen; (b) Aggregation of oxygen; (c) Escaping of oxygen; (d) Burst of oxygen

liquid silver [10,23]. The four formation stages of the pore finally lead to the situation that pores prefer to emerge in zone around the periphery of directly-contacting zone during the first 10000 operations. In addition, with the operation numbers increase, bubbles remaining inside molten pool will aggregate and reach the surface. Then, they burst due to the stronger tension. This is the reason why there is air hole to be observed in the central zone with larger operation numbers.

There is another possible explanation for the pores caused by solid particle splashing. According to the molten pool velocity field model [10], the zone with the fastest flow velocity of the molten pool at the arc root boundary is the periphery zone, where splashing is more likely to occur. The splashing of molten metal weakens the binding force between solid particle and liquid silver, so finally the pores are observed when the solid particle is left.

4.2.2 Formation process of molten silver on anode and cathode

It can be found that the shape of the molten silver on cathode is mainly like piled plates with rather round edge stacking on each other while that on anode resembles crawling islands, where more protrusions are stretched out from the larger islands, as presented in Fig. 5. The droplet-like morphology is more common on anode than cathode as well. Here, the morphology difference of the molten silver on cathode and anode may originate from the Ni distribution and gravity action.

According to our previous work [5], the distribution of Ag and Ni on cathode and anode contacts should be different after arc erosion action, as presented in Fig. 10(a). It can be found that more Ni particles distribute on anode surface than on cathode, which also explains why there are more pores on anode. On cathode, Ni element mainly distributes on the bottom molten pool while Ag element mainly distributes inside molten pool due to the density difference and the gravity action. From the theory that Ni increases the work function [9], this distribution makes arc easier to be ignited on cathode. However, the distribution of Ni and Ag element is layer upon layer in the molten pool on anode, which can stabilize molten pool on anode since Ni is capable of restricting the molten metal from flowing, while the molten metal is easier to flow on cathode because of the poor influence of Ni distributing at the bottom of molten pool posing on cathode surface.

On cathode, the effect of gravity is strong enough to break the restriction effect of Ni particles, making the molten silver fall and form numbers of droplets, as presented in Fig. 10(b). These droplets

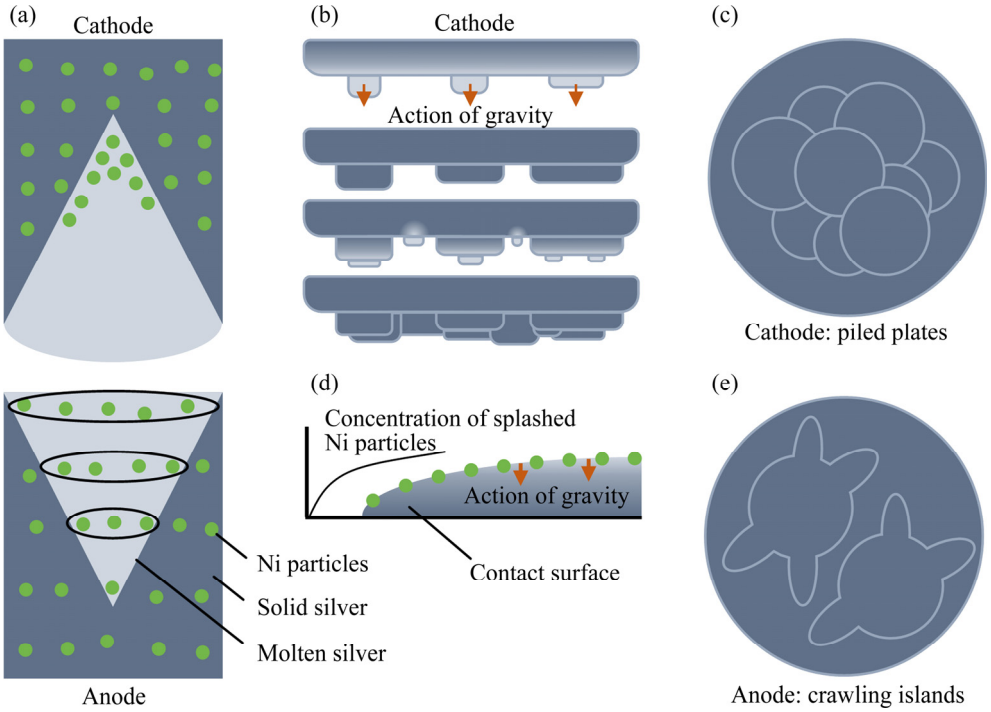

Fig. 10 Schematic of formation process of molten silver: (a) Ni and Ag distribution; (b) Action of gravity on cathode; (c) Piled plates on cathode; (d) Concentration of splashed Ni particles; (e) Crawling islands on anode

grow downward and extend horizontally in the meantime until they solidify into solid state as plates. When the thermal effect works on the contacts surface again, these newly formed plates will melt and part of them will begin to grow downward under the action of gravity again. The process described above repeats as the operation numbers increase, and the feature that molten silver is in the shape of piled plates on cathode becomes more and more obvious, as shown in Fig. 10(c).

Figure 10(d) indicates that the concentration of these splashed Ni particles is higher at the flat surface than the other parts, where the Ni particles are not much enough to stabilize the molten pool due to the low concentration. Meanwhile, the action of gravity will draw molten silver downward. Together with the negative temperature gradient on the direction perpendicular to the brink of the already solidified molten pool, molten silver is forced to flow only at the brink in the shape of protrusions, which resembles tentacles stretching out from islands, as depicted in Fig. 10(e).

All these factors above result in the difference of the molten silver morphology on anode and cathode. However, with the operation numbers increasing, the Ni particles that are capable of stabilizing molten pool are consumed in the form of splashing products too much, which makes it hard to have the molten pool restricted from flowing, and then the morphology of molten silver on anode and cathode becomes hard to distinguish from each other.

5 Conclusions

(1) With the increase of operation numbers, the arc erosion of Ag/10Ni electrical contact materials is more and more severe. With the same operation numbers, the arc erosion on anode is more serious than that on cathode. The mass gain on cathode should be mainly attributed to the molten bridge fracture and the mass loss on anode should be mainly attributed to the material transferring caused by arc erosion.

(2) The addition of Ni can stabilize the molten silver, prevent the the arc erosion and absorb the dissolved oxygen. However, the effect of Ni tends to disappear with the increase of operation numbers.

(3) The pores prefer to emerge around the arc effect spot during the first 10000 operations, whose formation process is influenced by the addition of Ni.

(4) The features of the molten silver on cathode and anode are piled plates and crawling islands, respectively, where the difference mainly originates from the action of gravity and the modifying effect of Ni for arc erosion.

Acknowledgments

This work was supported by the National Natural Science Foundation of China (No. 51601225), and Hunan Provincial Natural Science Foundation, China (No. 2020JJ5742).

References

[1] GUZMAN D, AGUILAR C, ROJAS P, CRIADO J M, DIANEZ M J, ESPINOZA R, GUZMAN A, MARTINEZ C. Production of Ag−ZnO powders by hot mechanochemical processing [J]. Transactions of Nonferrous Metals Society of China, 2019, 29(2): 365−373.

[2] XI Yong, WANG Xian-hui, ZHOU Zi-jing, LI Hang-yu, GUO Xiu-hua. Material transfer behavior of $AgTiB_2$ contact under different contact forces and electrode gaps [J]. Transactions of Nonferrous Metals Society of China, 2019, 29(5): 1046−1056.

[3] ZHANG Miao, WANG Xian-hui, YANG Xiao-hong, ZOU Jun-tao, LIANG Shu-hua. Arc erosion behaviors of $AgSnO_2$ contact materials prepared with different SnO_2 particle sizes [J]. Transactions of Nonferrous Metals Society of China, 2016, 26(3): 783−790.

[4] RAY N, KEMPF B, MÜTZEL T, HERINGHAUS F, FROYEN L, VANMEENSEL K, VLEUGELS J. Effect of Ni addition on the contact resistance of Ag−WC electrical contacts [J]. Journal of Alloys and Compounds, 2016, 670: 188−197.

[5] WU Chun-ping, YI Dani-qing, WENG Wei, LI Su-hua, ZHOU Jie-min, ZHENG Feng. Arc erosion behavior of Ag/Ni electrical contact materials [J]. Materials & Design, 2015, 85: 511−519.

[6] LIN Zhi-jie, LIU Shao-hong, LI Ji-guang, CHEN Jia-lin, XIE Ming, LI Xiao-dong, ZHANG Mu, ZHU Qi, HUO Di, SUN Xu-dong. Morphology-controllable synthesis and thermal decomposition of Ag and Ni oxalate for Ag−Ni alloy electrical contact materials [J]. Materials & Design, 2016, 108: 640−647.

[7] LI Ai-kun, ZHOU Wen-yan, XIE Ming, WANG Song, WANG Sai-bei, YANG You-cai, CHEN Yong-tai, LIU Man-men. Preparation and arc erosion behavior of AgNi10 contact material with different allotropes of carbon addition [J]. Diamond and Related Materials, 2021, 111: 1−11.

[8] MESSAOUD A, FAZEL N, GAROUX L, GASSER F, BEN YOUNES R, GASSER J G. A new high temperature design to determine electrical and thermal conductivities and thermoelectric power: Applications to the sintered composite

AgNi (90/10) “pseudo-alloy” [J]. Journal of Alloys and Compounds, 2018, 739: 407−417.
[9] LI Hang-yu, WANG Xian-hui, XI Yong, ZHU Ting, GUO Xiu-hua. Effect of Ni addition on the arc-erosion behavior of $AgTiB_2$ contact material [J]. Vacuum, 2019, 161: 361−370.
[10] WU Xi-xiu, LI Zhen-biao. Model on sputter erosion of electrical contact material [C]//48th IEEE Holm Conference on Electrical Contacts. Cpmt IEEE, 2002. 29−34.
[11] GUAN Wei-ming, YONG Pan, ZHANG Kun-hua, GUO Jun-mei. First principle study on the interface of Ag−Ni composites [J]. Rare Metal Materials and Engineering, 2010, 39(8): 1339−1343.
[12] UDAYABHASKAR R, SREEKANTH P, KARTHIKEYAN B. Optical and nonlinear optical limiting properties of AgNi alloy nanostructures [J]. Plasmonics, 2016, 11(6): 1461−1466.
[13] EL BEKRI T, CHAÂBANE L, CARVOU E. Experimental study of opening arcs in air of AgNi contacts [J]. International Journal of Materials Engineering Innovation, 2014, 5(4): 316−326.
[14] LAI Yi-jian, LIU Nan, WANG Yi-xu, ZHAO Bi-yuan, LI Jia. Research on failure features and protection methods of AgNi electrical contactor [C]//Proceedings of the 5th International Conference on Reliability of Electrical Products and Electrical Contacts, ICREPEC 2014. Wenzhou, China, 2014: 376−379.
[15] LI Hang-yu, WANG Xian-hui, HU Zhu-dong, GUO Xiu-hua. Investigation on arc behavior of AgNi electrical contact material with three-dimensional network structure [J]. Vacuum, 2020, 175: 1−13.
[16] WU Chun-Ping, YI Dani-qing, WEI Weng, LI Su-hua, ZHOU Jie-min. Influence of alloy components on arc erosion morphology of Ag/MeO electrical contact materials [J]. Transactions of Nonferrous Metals Society of China, 2016, 26(1): 185−195.
[17] WU Chun-ping, YUAN Meng, WU Qiong, XU Guo-fu, LIANG Xiao-peng, ZHAO Qian, LIU Hui-qun. Influence of $La_2Sn_2O_7$ on wetting behavior of Ag/SnO_2 composite materials [J]. Journal of Alloys and Compounds, 2020, 826: 1−12.
[18] YANG Fang-er, WANG Gui-cong, MU Cheng-fa, WU Jun-chen, SHEN Tao, ZHANG Ling-jie, ZHENG Xiao-hua. Microstructure and properties of MeO doped Ag/SnO_2 electric contact materials [J]. Rare Metal Materials and Engineering, 2020, 49(4): 1301−1305.
[19] LIN Zhi-jie, LIU Shao-hong, SUN Xu-dong, XIE Ming, LI Jia, LI Xiao-dong, CHEN Yong-tai, CHEN Jia-lin, HUO Di, ZHANG Mu, ZHU Qi, LIU Man-men. The effects of citric acid on the synthesis and performance of silver−tin oxide electrical contact materials [J]. Journal of Alloys and Compounds, 2014, 588: 30−35.
[20] LIN Zhi-jie, FAN Si-yu, LIU Man-men, LIU Shao-hong, LI Ji-guang, LI Jun-peng, XIE Ming, CHEN Jia-lin, SUN Xu-dong. Excellent anti-arc erosion performance and corresponding mechanisms of a nickel-belt-reinforced silver-based electrical contact material [J]. Journal of Alloys and Compounds, 2019, 788: 163−171.
[21] WU Chun-ping, ZHAO Qian, LI Na-na, WANG Hai-sheng, YI Dan-qing, WENG Wei. Influence of fabrication technology on arc erosion of $Ag/10SnO_2$ electrical contact materials [J]. Journal of Alloys and Compounds, 2018, 766: 161−177.
[22] XU Guo-fu, HUANG Run-zhang, YUAN Meng, WU Qiong, WU Chun-ping. Influence of operation numbers on arc erosion behavior of Ag/ZnO electrical contact materials [J]. The Chinese Journal of Nonferrous Metals, 2021, 31(5): 1285−1298. (in Chinese)
[23] LI Zhen-biao, WU Xi-xiu, NOURI H, HASEGAWA M. Sputter erosion model of arcing contact materials [J]. IEICE Transactions on Electronics, 2007, 90(7): 1356−1360.

操作次数对 Ag/Ni 电触头材料电弧侵蚀行为的影响

黄润章[1]，徐国富[1,2]，吴 琼[1]，元 梦[1]，吴春萍[1,2]

1. 中南大学 材料科学与工程学院，长沙 410083；
2. 中南大学 有色金属材料科学与工程教育部重点实验室，长沙 410083

摘 要：使用金相显微镜，三维轮廓仪以及扫描电子显微镜对 Ag/Ni 电触头材料在不同操作次数下的电弧侵蚀行为进行研究。结果显示，通过烧结−挤压工艺制备的 Ag/10Ni 电触头材料在操作次数从 1000 增加至 40000 的过程中电弧侵蚀现象呈现愈发严重的趋势。在相同操作次数下，阳极表面电弧侵蚀比阴极表面更加明显。在最初的 10000 次接触操作中，气孔倾向于出现在电弧接触点周围。熔银在阴极与阳极表面的形貌差异则来自于重力以及电弧侵蚀的影响。此外，讨论电弧能量、电弧时间、熔焊力、接触电阻、温度以及触头质量变化之间的关系，结果表明：阴极表面质量变化主要由熔桥断裂引起。

关键词：Ag/Ni 电触头材料；操作次数；电弧侵蚀；电弧参数

(Edited by Bing YANG)